Experimental Characterization and Numerical Modeling of Spatially Distributed Viscoelasticity in Short-Fiber-Reinforced Composite Tensile-Test Specimens

E. Klatt[1*] and N. Rauter[1]

[1] Helmut-Schmidt-University / University of the Federal Armed Forces, Chair of Solid Mechanics, Holstenhofweg 85, 22043 Hamburg, Germany

* *Corresponding author (eduard.klatt@hsu-hh.de)*

Keywords: *short-fiber-reinforced composite; digital image correlation; nanoindentation; random fields; expansion optimal linear estimation method*

1. Abstract

Injection-molded short-fiber-reinforced composites exhibit spatially heterogeneous and time-dependent behavior due to interactions between matrix viscoelasticity and process-induced fiber microstructure. This work presents an experimentally validated stochastic framework for modeling spatially distributed viscoelasticity in tensile specimens of short-fiber-reinforced composites. Two material systems, unreinforced PBT GF0 and short-fiber-reinforced PBT GF30, were investigated to distinguish matrix-dominated viscoelasticity from fiber-induced spatial variability. At the component scale, digital image correlation was used to measure local strain histories at 15 regions along the gage section. At the microscale, nanoindentation on polished cross-sections quantified local creep-related indentation responses. PBT GF0 demonstrates largely homogeneous behavior, while PBT GF30 displays pronounced spatial scatter at both scales. To represent this variability, apparent viscoelastic parameters are modeled as second-order Gaussian random fields and discretized using the expansion optimal linear estimate method. Comparison with experimental creep data indicates that the stochastic model accurately reproduces the observed strain range and spatial patterns of the component-level response. This framework enables the integration of measured spatial variability into numerical simulations of short-fiber-reinforced composites.

2. Introduction

Injection-molded short-fiber-reinforced composites (SFRC) are widely used in engineering applications due to their cost-effective mass production, high stiffness-to-weight ratio, and consistent performance. However, the injection molding process produces a heterogeneous microstructure characterized by spatial variations in fiber orientation, content, and length. Consequently, the mechanical behavior at the component level is spatially non-uniform and stochastic, with local material properties varying across the specimen. This variability leads to significant deformation gradients and localized strain under applied loads.

In addition to process-induced heterogeneity, polymer-based matrix systems exhibit pronounced time-dependent behavior. In SFRC, the polymer matrix primarily governs viscoelasticity, while the fibers influence both its magnitude and spatial distribution. This interaction is particularly significant under sustained loading, where local stiffness and viscoelastic variations affect overall deformation. Therefore, reliable prediction of SFRC structural response requires an accurate viscoelastic constitutive model and a comprehensive description of spatial variability in material parameters.

Random fields offer an appropriate framework for modeling spatially varying constitutive parameters as realizations of stochastic fields, with their statistics defined by experimentally or numerically determined correlation functions. This methodology captures local material responses without the need to explicitly resolve individual fibers in component-scale simulations. In this study, spatially distributed linear viscoelastic behavior is represented using a single-term Prony series with spatially varying parameters, and stochastic discretization is achieved through a spectral representation method that generates random-field realizations consistent with the identified correlation structure.

This study integrates component- and microscale experimental approaches. At the component level, digital image correlation (DIC) is employed to measure spatial strain fields in tensile specimens under load. At the microscale, nanoindentation is used to characterize local viscoelastic responses across polished cross-sections. These complementary methods reveal spatial variability in viscoelastic properties and provide the foundation for subsequent stochastic modeling. Comparative analysis of unreinforced and short-fiber-reinforced materials explains the influence of short fibers on local variations in viscoelastic behavior.

This paper introduces an experimentally validated and computationally efficient framework for characterizing and modeling spatially distributed viscoelasticity in injection-molded SFRC tensile specimens. Local viscoelastic behavior is initially measured experimentally at both the component and microscale levels. The spatial variability of Prony-series constitutive parameters is subsequently modeled using second-order random fields, which are incorporated into a two-dimensional numerical model of the specimen. Numerical results are then compared with experimental data to evaluate the framework's ability to reproduce observed spatial trends in structural response.

3. Modeling framework

3.1. Linear viscoelastic constitutive representation

Creep refers to the time-dependent deformation observed in materials under constant load and temperature, constituting a primary manifestation of viscoelastic behavior in polymeric materials [11]. The total strain as a function of time is expressed as the sum of an instantaneous elastic component and a time-dependent creep component,

$$\varepsilon(\mathrm{t}) = \varepsilon_{\mathrm{total}}(t) = \varepsilon_{\mathrm{linear\ elastic}} + \varepsilon_{\mathrm{creep}}(t)\,. \tag{1}$$

Creep characterizes material behavior under constant stress, whereas stress relaxation describes the response under constant strain. The constitutive modeling of general linear viscoelasticity, which encompasses both phenomena, employs rheological elements as illustrated in Figure 1. The spring models the elastic response with stiffness K_{eq} in accordance with Hooke's law, while the dashpot represents purely viscous behavior with dynamic viscosity η as described by Newton's law. A Maxwell element is formed by connecting a spring and a dashpot in series. The generalized Maxwell model is constructed by placing an equilibrium spring K_{eq} in parallel with N_i Maxwell elements.

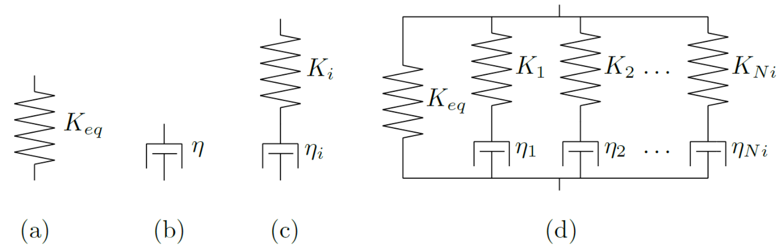

Figure 1. Rheological elements used for the description of linear viscoelasticity: a) spring with stiffness K_{eq}, b) dashpot, c) Maxwell element, and d) generalized Maxwell model [6].

When $N_i = 1$ in the generalized Maxwell model (commonly termed the standard linear solid), the stress–strain relationship is governed by a first-order differential equation [11], given by

$$\frac{\mathrm{d}\sigma(t)}{\mathrm{d}t} + \frac{K_1}{\eta_1}\sigma(t) = \left(K_{\text{eq}} + K_1\right)\frac{\mathrm{d}\varepsilon(t)}{\mathrm{d}t} + \frac{K_{\text{eq}}K_1}{\eta_1}\varepsilon(t)\,. \tag{2}$$

The Prony series provides a convenient mathematical representation of time-dependent relaxation behavior, corresponding to the solution of the underlying ordinary differential equations. The relaxation function is expressed as

$$K(t) = K_{\text{eq}} + \sum_{i=1}^{N_i} K_i\, e^{-t/\tau_i}\,, \tag{3}$$

where K_{eq} and K_1 represent the equilibrium stiffness and the relaxation amplitudes of the i-th branch, respectively. The parameter $\tau_i = \eta_i/K_i$ defines the characteristic relaxation time for each Maxwell element. In practice, the parameters of the Prony series are identified by fitting the model to experimental data [7].

3.2. Random-field representation of spatially varying material properties

Spatial variations in constitutive parameters are modeled as random fields. Extending a random variable $Z(\omega)$ to include the spatial coordinate $\boldsymbol{x}$ over the domain yields

$$Z(\boldsymbol{x}) = Z(\omega, \boldsymbol{x})\,. \tag{4}$$

A Gaussian random field is defined by its mean $\mu(\boldsymbol{x})$, standard deviation $\sigma(\boldsymbol{x})$, and correlation coefficient $\rho(\boldsymbol{x}_1, \boldsymbol{x}_2)$. The correlation coefficient is related to the covariance by

$$\rho_{12} = \rho_{Z_1,Z_2} = \frac{\mathrm{Cov}[Z_1, Z_2]}{\sigma_1\sigma_2}\,. \tag{5}$$

In this study, the random fields are assumed to be second-order homogeneous. Therefore, the mean and standard deviation are constant, and the correlation structure depends solely on the relative coordinate vector $\boldsymbol{\xi}$.

For numerical generation, the expansion optimal linear estimation (EOLE) method is employed [8]. Based on the covariance matrix

$$C(\boldsymbol{x}_1, \boldsymbol{x}_2) = \rho(\xi_1, \xi_2)\,, \tag{6}$$

the discrete eigenvalue problem

$$\boldsymbol{C}\,\boldsymbol{\phi}_n = \lambda_n\,\boldsymbol{\phi}_n \tag{7}$$

is solved. The truncated random field is then given by

$$\hat{Z}(\omega, \boldsymbol{x}) = \mu + \sum_{n=1}^{M} \sqrt{\lambda_n}\,\phi_n(\boldsymbol{x}) Z_n(\omega)\,. \tag{8}$$

The spatial discretization used for the random-field representation is shown schematically in Figure 2. The tensile-test specimen is reduced to a two-dimensional computational domain, on which the stochastic field is evaluated at predefined discretization points.

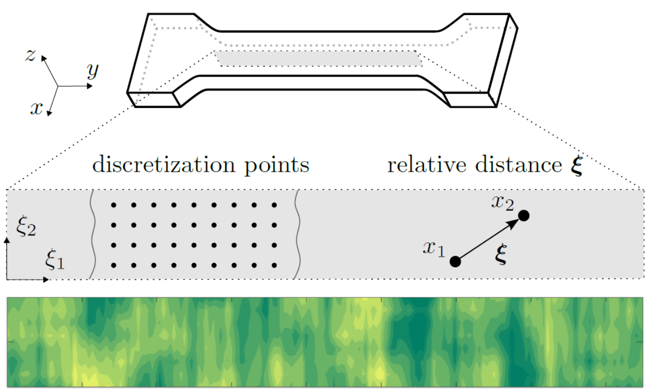

Figure 2. Schematic representation of the random-field discretization for the tensile-test specimen. The component geometry is simplified to a two-dimensional domain, where discretization points are defined for stochastic field representation. The relative distance vector $\boldsymbol{\xi} = \boldsymbol{x}_2 - \boldsymbol{x}_1$ between two spatial positions $\boldsymbol{x}_1$ and $\boldsymbol{x}_2$ determines the correlation structure. An example of a numerically generated second-order Gaussian random field is depicted below the discretized domain [6].

3.3. Multiscale framework based on statistical volume elements

The classical multiscale concept is based on a Representative Volume Element (RVE), which must be sufficiently large to represent the statistical features of the heterogeneous microstructure while remaining sufficiently small compared with the macroscopic structural dimensions [2, 9]. Under these idealized conditions, homogenization yields unique effective material properties. For random microstructures in finite domains, however, this classical RVE concept is generally not fulfilled in engineering practice. Instead, the mesoscale response is characterized by Statistical Volume Elements (SVEs), whose constitutive behavior strongly depends on the specific microstructural realization, the chosen window size with a characteristic length scale d_δ, and the applied boundary conditions [5, 9, 10]. This conceptual multiscale framework and the systematic extraction of SVEs are schematically illustrated in Figure 3.

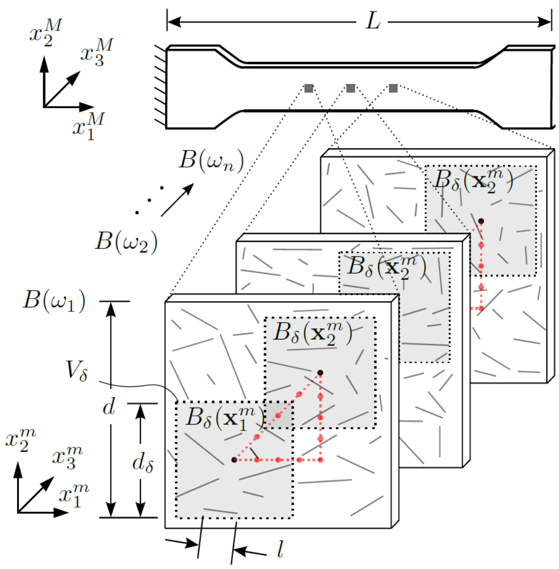

Figure 3. Schematic representation of the multiscale framework based on SVEs. At the component level, a tensile-test specimen with characteristic length L is considered, while the heterogeneous microstructure is modeled by an ensemble of realizations $B(\omega_1), B(\omega_2), \ldots, B(\omega_n)$. Within each realization, local subdomains $B_\delta(\boldsymbol{x}_1^m)$ and $B_\delta(\boldsymbol{x}_2^m)$ of characteristic size d_δ are extracted as SVEs. The microstructural length scale is denoted by l. The apparent constitutive response of these SVEs forms the basis for spatially resolved material descriptions at the component scale.

The scale transition follows Hill's macrohomogeneity condition [4], which asserts energetic equivalence between the local microscopic response and the homogenized mesoscopic response, expressed as

$$\langle \boldsymbol{\sigma} : \boldsymbol{\varepsilon} \rangle_\delta = \langle \boldsymbol{\sigma} \rangle_\delta : \langle \boldsymbol{\varepsilon} \rangle_\delta \,. \tag{9}$$

For a finite SVE, the resulting constitutive quantities are considered apparent properties rather than effective properties in the strict homogenization sense [5]. In the linear-elastic reference case, the apparent constitutive response at the window center $\boldsymbol{x}^m$ is given by

$$\langle \boldsymbol{\sigma}(\boldsymbol{x}^m, \omega) \rangle_\delta = \mathbb{C}_\delta^{\text{app}}(\boldsymbol{x}^m, \omega) : \langle \boldsymbol{\varepsilon}(\boldsymbol{x}^m, \omega) \rangle_\delta \,, \tag{10}$$

or, equivalently,

$$\langle \boldsymbol{\varepsilon}(\boldsymbol{x}^m, \omega) \rangle_\delta = \mathbb{S}_\delta^{\text{app}}(\boldsymbol{x}^m, \omega) : \langle \boldsymbol{\sigma}(\boldsymbol{x}^m, \omega) \rangle_\delta \,. \tag{11}$$

In the time-dependent case, the mesoscale constitutive response is described by apparent viscoelastic constitutive tensors. Accordingly, the apparent stress response of the SVE is expressed in hereditary integral form as

$$\langle \boldsymbol{\sigma}(\boldsymbol{x}^m, t, \omega) \rangle_\delta = \int_0^t \mathbb{C}_\delta^{\text{app}}(\boldsymbol{x}^m, t - \tau, \omega) : \frac{\partial \langle \boldsymbol{\varepsilon}(\boldsymbol{x}^m, \tau, \omega) \rangle_\delta}{\partial \tau} \, \mathrm{d}\tau \,. \tag{12}$$

The local apparent viscoelastic response is computationally approximated using a one-term Prony series. As a result, the spatially varying constitutive behavior of the heterogeneous material is characterized by apparent parameter fields instead of unique effective constants.

These fields are obtained using the moving-window method [1, 3]. A window of specified size d_δ is systematically moved across a larger microstructural realization, with each extracted subdomain treated as an individual SVE. The apparent viscoelastic parameters determined for each window are assigned to the corresponding geometric window centers, yielding spatially resolved parameter fields,

$$\boldsymbol{\Theta}^{\mathrm{app}} = \boldsymbol{\Theta}^{\mathrm{app}}(\boldsymbol{x}^m)\,. \tag{13}$$

These discrete fields form the basis for subsequent correlation analysis and for the stochastic representation of apparent viscoelastic material behavior as continuous random fields at the component scale [7, 10].

4. Materials and experimental methods

4.1. Material systems and specimen manufacturing

Two injection-molded thermoplastic material systems were investigated to distinguish the intrinsic viscoelastic response of the polymer matrix from the additional spatial variability induced by short-fiber reinforcement. The reference material was unreinforced polybutylene terephthalate (PBT), designated as PBT GF0. The reinforced material system consisted of PBT with a fiber mass fraction of 30%, designated as PBT GF30. The matrix material is commercially available as ULTRADUR B 4520 from BASF. The reinforcement phase consisted of short E-glass fibers, designated as FGCS 3540 and supplied by STW.

Standardized tensile-test specimens according to DIN EN ISO 527-2 type 1A were manufactured by injection molding at Kunststoff-Zentrum Leipzig gGmbH. Identical specimen geometry and processing conditions were used for both material systems, enabling a direct comparison between the matrix-dominated response of the unreinforced polymer and the heterogeneous response of the SFRC. Consequently, PBT GF0 served as a reference material, whereas PBT GF30 was used to assess the influence of process-induced microstructural heterogeneity on local viscoelastic material behavior.

4.2. Component-level characterization by DIC

The spatially resolved deformation of the tensile specimens under load was analyzed using DIC. Instead of using only global engineering strain, the surface deformation field over the gage section was recorded and evaluated locally. This allowed detection of spatially varying strain and direct experimental access to the non-uniform viscoelastic response at the specimen scale.

The gage section was divided into 15 local regions (Figure 4), each with an initial length of $l_0 = 5\ mm$ along the specimen axis. Local strain evolution in these regions was derived from DIC data to quantify the spatial distribution of time-dependent deformation along the specimen length.

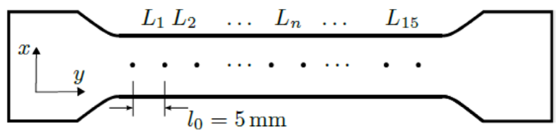

Figure 4. Schematic division of the tensile-test specimen's gage section into 15 local regions $L_1, L_2, \ldots, L_{15}$, each with an initial length $l_0 = 5$ mm used for local strain evolution analysis from DIC measurement [6].

The resulting local strain histories formed the basis for assessing spatial scatter at the component level and allowed direct comparison of experimentally observed deformation patterns with stochastic model predictions.

4.3. Microscale characterization by nanoindentation

At the microscale, nanoindentation was used to characterize the local viscoelastic response on polished specimen cross-sections. Small samples taken from the tensile specimens were embedded if necessary and sequentially ground and polished to obtain a smooth x-z cross-sectional surface for testing (Figure 5). Indentation was performed with an instrumented nanoindenter using a Berkovich tip and a load–hold–unload protocol. The increase in indentation depth during the hold segment served as a local measure of viscoelastic creep.

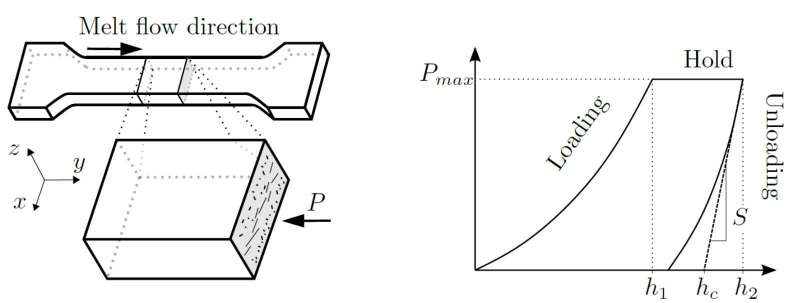

Figure 5. Schematic of the nanoindentation method. A small specimen is cut from the tensile-test sample, and its polished x-z cross-section is used for indentation. The applied load–hold–unload sequence is shown schematically, with the hold segment enabling assessment of time-dependent indentation behavior.

Nanoindentation measurements were performed at multiple positions across the polished cross-section to map spatial variability in the local response. The evaluation focused on a creep-related indentation parameter derived from the depth increase during the holding segment, which served as a local measure for comparing the microscale viscoelastic responses of the unreinforced and short-fiber-reinforced materials.

5. Experimental observations of spatially distributed viscoelasticity

5.1. Component-level observations from DIC

At the component level, local deformation was evaluated in 15 predefined regions along the gage section. The resulting strain histories describe the spatially resolved, time-dependent deformation under tensile loading and reveal local deviations from the global specimen response due to spatial scatter in viscoelastic behavior.

To obtain a compact parameter-based description of the local time-dependent response, the strain histories of each region were fitted using the single-term Prony series in Equation 3. The resulting local stiffness parameter K_i is shown in Figure 6 for one representative specimen of each material system and compared with the global mean value from the full 75 mm gage section, averaged over 20 specimens.

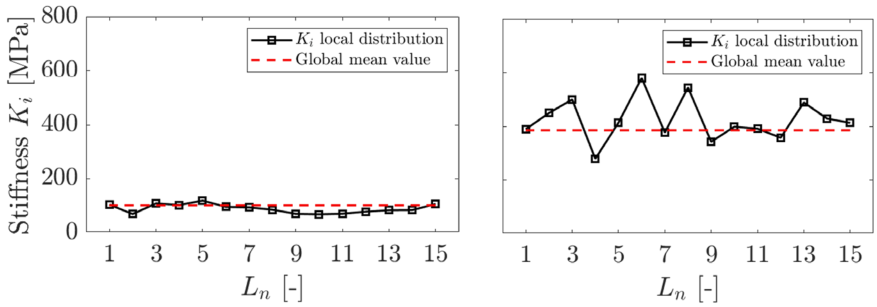

Figure 6. Local distribution of the Prony stiffness parameter K_1 across the 15 evaluation regions L_n of the tensile-test specimen at the component level: PBT GF0 is shown on the left, and PBT GF30 is shown on the right.

For PBT GF0, the local stiffness parameter K_i varies only slightly along the specimen axis, indicating that the component-level viscoelastic response of the unreinforced material is mainly governed by a relatively homogeneous polymer matrix. In contrast, PBT GF30 exhibits a highly non-uniform spatial distribution of K_i, with local deviations from the global mean due to process-induced fiber architecture, including variations in fiber orientation, content, and length. As a result, the reinforced material exhibits much larger local fluctuations than the unreinforced reference, showing that its component-level viscoelastic behavior cannot be captured by a single spatially homogeneous parameter set.

5.2. Microscale observations from nanoindentation

At the microscale, nanoindentation was performed on polished x-z cross-sections of the tensile specimens. The creep-related indentation parameter $Creep = h_2 - h_1$, obtained from the hold segment of the load-hold-unload protocol, was used as a local measure of time-dependent material response, enabling direct evaluation of spatial viscoelastic variability across the cross-section. Figure 7 shows the spatial distributions of $Creep$ for PBT GF0 and PBT GF30, based on 160 indentation points per material. The unreinforced PBT GF0 exhibits a comparatively uniform distribution of the creep-related parameter.

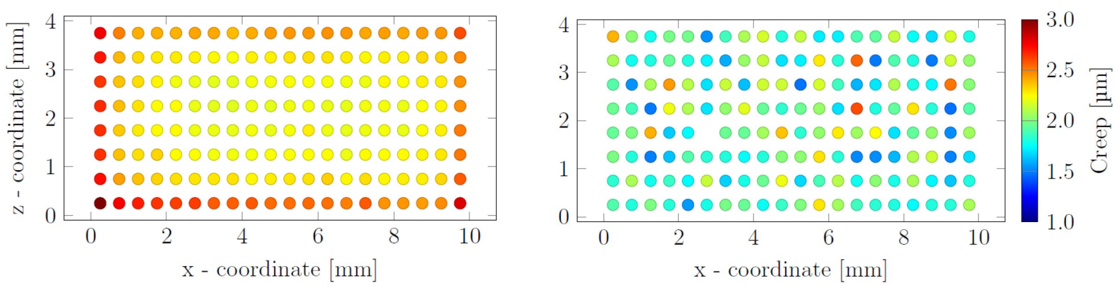

Figure 7. The creep value of 160 measurement points over the cross-section shows the unreinforced material PBT GF0 on the left side and the short-fiber-reinforced material PBT GF30 on the right side [6].

In contrast, PBT GF30 shows a clearly more heterogeneous $Creep$ distribution. Local variations in indentation response arise from the spatial fiber arrangement, adjacent matrix regions, and the layered morphology of injection-molded parts. Compared with PBT GF0, the reinforced material exhibits markedly increased microscale scatter, confirming that short-fiber reinforcement enhances the local variability of the viscoelastic response.

Together with the component-level DIC observations, the nanoindentation results show spatial variability at both investigated scales. PBT GF0 serves as a relatively homogeneous, matrix-dominated reference, whereas PBT GF30 exhibits pronounced local scatter due to process-induced microstructural heterogeneity. These findings justify treating apparent viscoelastic parameters as spatially distributed random fields in the subsequent numerical analysis.

6. Numerical implementation and comparison with experiments

The stochastic material description was implemented by assigning spatially varying apparent viscoelastic parameters to the two-dimensional tensile-specimen model. The random field was generated using the EOLE-based discretization in Section 3.2. The numerical response was evaluated over the same 15 local regions as in Figure 4, allowing direct comparison with the DIC-based experimental strain histories.

Figure 8 summarizes the numerical implementation and comparison with experimental creep data for PBT GF30. The left diagram shows selected time-dependent apparent stiffness responses $C_{11}^{\delta}(t)$ from different SVE realizations, while the right diagram compares the corresponding numerical strain histories with the measured local creep responses. The numerical model reproduces the experimental strain range and captures the spatially distributed viscoelastic response at the component level.

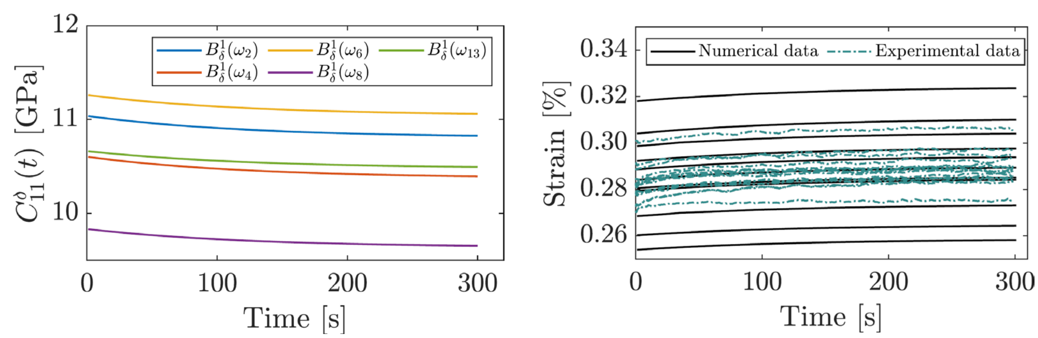

Figure 8. Numerical implementation and comparison with experimental observations for PBT GF30: on the left side, the time-dependent apparent stiffness responses $C_{11}^{\mathrm{app}}(t)$ from selected SVE realizations, while on the right side, the comparison of numerical strain histories with experimental DIC-based creep data from 15 local regions of the tensile specimen [6].

7. Conclusions

This paper presents an experimentally validated stochastic modeling framework for spatially distributed viscoelasticity in injection-molded SFRC tensile specimens. Experiments at component and microscale levels show that the presence and spatial arrangement of short fibers strongly influence the local viscoelastic response. While unreinforced PBT GF0 exhibits nearly homogeneous, matrix-dominated behavior, reinforced PBT GF30 shows pronounced spatial scatter due to the process-induced microstructure.

The results show that a single spatially homogeneous parameter set cannot describe the viscoelastic response. Instead, the local behavior is better captured by apparent viscoelastic parameters that vary over the specimen domain. Second-order Gaussian random fields are used for the spatial distribution of constitutive parameters, and an EOLE discretization yields an efficient finite-dimensional representation.

Numerical comparisons with creep experiments demonstrate that the proposed stochastic model reproduces the observed range and spatial trends of component-level deformations. The approach thus provides a basis for incorporating experimentally observed spatial variability into numerical simulations of short-fiber-reinforced composites. Future work should address larger specimen sets, additional loading conditions, and experimental identification of correlation lengths from DIC data.

8. References

[1] S.C., Baxter, L.L., Graham. "*Characterization of random composites using moving-window technique*". Journal of Engineering Mechanics, Vol. 126, No. 4, pp 389-397, 2000.

[2] I.M. Gitman, H. Askes, L.J. Sluys. "*Representative volume: Existence and size determination*". Engineering Fracture Mechanics, Vol. 74, No. 16, pp 2518–2534, 2007

[3] L.L. Graham-Brady, E.F. Siragy, S.C. Baxter. "*Analysis of heterogeneous composites based on moving-window techniques*". Journal of Engineering Mechanics, Vol. 129, No. 9, pp 1054–1064, 2003

[4] R. Hill. "*Elastic properties of reinforced solids: Some theoretical principles*". Journal of the Mechanics and Physics of Solids, Vol. 11, No. 5, pp 357–372, 1963

[5] C. Huet. "*Application of variational concepts to size effects in elastic heterogeneous bodies*". Journal of the Mechanics and Physics of Solids, Vol. 38, No. 6, pp 813–841, 1990

[6] E. Klatt, N. Rauter. "*Stochastic modelling of the spatially distributed viscoelasticity of short fiber-reinforced composites using random fields*". Proceedings of the 24th International Conference on Composite Materials (ICCM24), 2025

[7] E. Klatt, B. Zimmering, O. Niggemann, N. Rauter. "A comparative characterization of the creep behavior of short-fiber reinforced composites based on the Prony series and fractional derivative-based creep models". Applied Mechanics, Vol. 6, No. 3, pp 2673-3161, 2025

[8] C.-C. Li, A. Der Kiureghian. "*Optimal discretization of random fields*". Journal of Engineering Mechanics, Vol. 119, No. 6, pp 1136–1154, 1993

[9] M. Ostoja-Starzewski. "*Material spatial randomness: From statistical to representative volume element*". Probabilistic Engineering Mechanics, Vol. 21, No. 2, pp 112–132, 2006

[10] N. Rauter, R. Lammering. "*Correlation structure in the elasticity tensor for short fiber-reinforced composites*". Probabilistic Engineering Mechanics, Vol. 62, 2020

[11] N.W. Tschoegl. "*The Phenomenological Theory of Linear Viscoelastic Behavior: An Introduction*". Springer, 1989